The lung vascular filter as a site of immune induction for T cell responses to large embolic antigen

Monique A.M. Willart,[1] Hendrik Jan de Heer,[2] Hamida Hammad,[1] Thomas Soullié,[2] Kim Deswarte,[1] Björn E. Clausen,[3] Louis Boon,[4] Henk C. Hoogsteden,[2] and Bart N. Lambrecht[1,2]

[1]Laboratory of Immunoregulation and Mucosal Immunology, Department of Pulmonary Medicine, University of Ghent, Ghent B-9000, Belgium
[2]Department of Pulmonary Medicine and [3]Department of Immunology, Erasmus Medical Center, Rotterdam 3000 CA, Netherlands
[4]Bioceros B.V., Utrecht 3584 CM, Netherlands

The bloodstream is an important route of dissemination of invading pathogens. Most of the small bloodborne pathogens, like bacteria or viruses, are filtered by the spleen or liver sinusoids and presented to the immune system by dendritic cells (DCs) that probe these filters for the presence of foreign antigen (Ag). However, larger pathogens, like helminths or infectious emboli, that exceed 20 µm are mostly trapped in the vasculature of the lung. To determine if Ag trapped here can be presented to cells of the immune system, we used a model of venous embolism of large particulate Ag (in the form of ovalbumin [OVA]–coated Sepharose beads) in the lung vascular bed. We found that large Ags were presented and cross-presented to CD4 and CD8 T cells in the mediastinal lymph nodes (LNs) but not in the spleen or liver-draining LNs. Dividing T cells returned to the lungs, and a short-lived infiltrate consisting of T cells and DCs formed around trapped Ag. This infiltrate was increased when the Toll-like receptor 4 was stimulated and full DC maturation was induced by CD40 triggering. Under these conditions, OVA-specific cytotoxic T lymphocyte responses, as well as humoral immunity, were induced. The T cell response to embolic Ag was severely reduced in mice depleted of CD11c^{hi} cells or Ly6C/G^{+} cells but restored upon adoptive transfer of Ly6C^{hi} monocytes. We conclude that the lung vascular filter represents a largely unexplored site of immune induction that traps large bloodborne Ags for presentation by monocyte-derived DCs.

CORRESPONDENCE
Bart N. Lambrecht:
Bart.lambrecht@ugent.be

Abbreviations used: Ag, antigen; DT, diphtheria toxin; DTR, diphtheria toxin receptor; MCP-1, monocyte chemotactic protein 1; MLN, mediastinal LN; OB, OVA bead; pDC, plasmacytoid DC; PLN, peripheral LN; PPD, purified protein derivate; Tg, transgenic; UB, uncoated bead.

DCs are the most important APCs for mounting a primary immune response to foreign antigens (Ags) that invade the various barriers of the body such as the skin, gastrointestinal, and respiratory mucosae (Banchereau and Steinman, 1998). DCs have been well studied and their function is to take up Ag across the lining barrier, integrate signals on the pathogenicity of the Ag, and migrate via the afferent lymph to the regional draining LNs. In the T cell area of these draining LNs, DCs induce a tailor-made immune response that is optimal to clear the pathogen in the best possible way while avoiding damage to self (Banchereau and Steinman, 1998). Another portal of entry, but also a portal of dissemination of invading pathogens, is the bloodstream. Pathogens that reach the bloodstream, either through direct puncture of the skin or invasiveness through mucosal surfaces such as the nasopharynx or lung, are easily carried throughout the body. It is most often assumed that these Ags will be filtered by the splenic microarchitecture, particularly the splenic marginal zone, and subsequently presented by splenic DCs and/or macrophages to naive T cells for induction of a primary protective immune response (De Smedt et al., 1996; Morón et al., 2002). Some bloodborne pathogens might also be filtered and presented in the bone marrow (Feuerer et al., 2003). For pathogens that replicate and invade

M.A.M. Willart and H. Jan de Heer contributed equally to this paper.

The Rockefeller University Press $30.00
J. Exp. Med. Vol. 206 No. 12 2823-2835
www.jem.org/cgi/doi/10.1084/jem.20082401

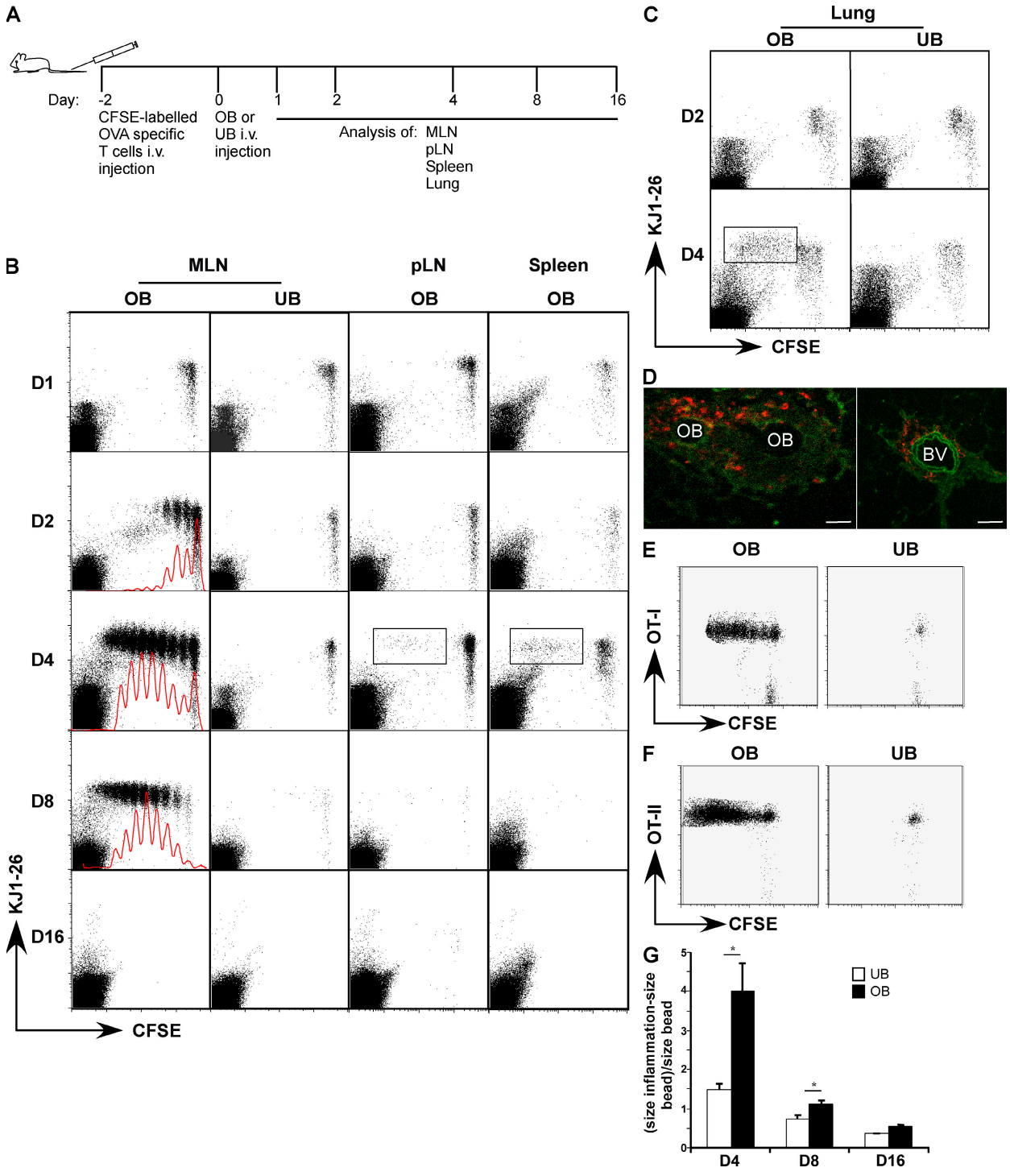

Figure 1. Embolic large particulate Ag in the lung is presented in draining MLNs. (A) BALB/c or C57BL/6 were injected with OVA-specific CFSE-labeled TCR Tg T cells 2 d before i.v. injection of particulate Ag ($OVA_{323-339}$ peptide, LPS-free OVA, or control glycine). At 1, 2, 4, 8, and 16 d after injection of particulate Ag, mice were sacrificed and MLNs, PLNs, spleen, and lungs were analyzed for a T cells response. This experiment was performed three times with four mice at each time point. (B) Response of OVA-specific CFSE-labeled $CD4^+$ DO11.10 T cells after injection of OBs or UBs at indicated days. MLNs, PLNs, and spleens were analyzed for the occurrence of OVA T cell division (CFSE profile, x axis) in OVA-specific $KJ1.26^+$ T cells (y axis). Recirculating divided T cells are indicated in rectangles. FACS plots represent a single animal of a group of five at each day point. The experiment was performed three times. (C) Division profile (CFSE, x axis) of KJ1-26 $CD4^+$ DO11.10 T cells (y axis) in the lung at 2 and 4 d after injection of OB or UB. Recirculating divided T cells are indicated in rectangles. FACS plots represent a single animal of a group of five at each day point. The experiment was performed three times. (D) Confocal imaging of frozen section of lungs stained with the OVA-specific TCR-specific marker KJ1-26 (red). At day 4 after injection of OBs,

the bloodstream via the gastrointestinal tract, the portal circulation can lead to filtering in the liver blood sinusoids and Ag presentation by DCs in liver draining LNs (Kudo et al., 1997).

Another, often neglected mechanism might exist in the lungs to filter bloodborne pathogens. The pulmonary vascular system with its small diameter arterioles (20–500-μm diameter) and capillaries (<10-μm diameter) forms an extensive meshwork that receives the complete cardiac output of blood (for comparison, the spleen receives only 5% of cardiac output or 200–300 ml/min). Large particles that circulate in the bloodstream (called emboli in the medical literature) and exceed the diameter of the small pulmonary vessels are very efficiently trapped by this system. It is currently unknown whether Ags or pathogens that clog the lung vascular system would be presented to the immune system in a way that leads to protective immunity, which is analogous to the splenic or liver filter system. The lung vascular bed is situated in the lung interstitium, where a well developed network of interstitial DCs and macrophages is present (GeurtsvanKessel and Lambrecht, 2008). However, APCs of the lung interstitium have generally been regarded as sessile cells that only stimulate already primed T cells, for example, during pulmonary delayed-type hypersensitivity reactions and granuloma formation (Holt et al., 1988; Gong et al., 1994; Iyonaga et al., 2002; Tsuchiya et al., 2002). DCs are also found to line the intima and adventitia of larger (pulmonary) vessel walls and, therefore, could probe the luminal contents for the presence of Ags, although it is unclear to what Ags this sampling system would react (Millonig et al., 2001; Perros et al., 2007; Choi et al., 2009).

The purpose of this study was to determine whether the lung vascular system allows Ag sampling and, thus, acts as a site of immune induction for T cell responses after i.v. injection of particulate Ag. For this, we injected large Sepharose beads coupled or not to ovalbumin (OVA). Because of their size (± 40–150 μm), i.v.-injected beads are specifically retained in the vascular bed of the lung. Our studies revealed a hitherto unexplored potential of $CD11c^+$ DCs and their immediate monocytic precursors to sample the lung vascular compartment for trapped Ag, leading to Ag presentation in lung draining LNs and generation of effector responses to OVA.

RESULTS

Embolic large particulate Ag is presented and cross-presented exclusively in the mediastinal LNs (MLNs) draining the lung

We i.v. injected large Sepharose beads coupled or not to $OVA_{323-339}$ peptide (coded, respectively as OVA beads [OBs] and uncoated beads [UBs]), the immunodominant MHCII-restricted peptide of OVA. To allow detection of the precise site of primary T cell activation and division, 2 d earlier, mice received a cohort of CFSE-labeled $CD4^+$ OVA TCR transgenic (Tg) DO11.10 T cells (Fig. 1 A), recognizing the $OVA_{323-339}$ peptide in the context of $I\text{-}A^d$ (MHCII). The precise localization and degree of T cell proliferation, as measured by sequential halving of CFSE intensity with each round of T cell division, was measured over time in different anatomical compartments, including the lung, draining MLN, peripheral nondraining LN, and spleen, up until 16 d after bead injection. Proliferation of naive OVA-specific T cells first occurred exclusively in draining MLNs of the lung 2 d after injection of OBs but not after injection of UBs (Fig. 1 B). Despite the i.v. injection of Ag, no divisions were observed in spleen or nondraining peripheral LNs (PLNs), illustrating that free or particle-bound Ag did not leak from trapped Ag or pass beyond the lung capillary filter. More specifically, we also tested whether primary divisions were found in the liver draining LNs yet found no evidence for this (Fig. S1). When we focused on the lung interstitium itself, which was obtained by enzymatic digestion of a lung lobe, we could not detect divided T cells 2 d after injection of beads (Fig. 1 C). When the T cell response was followed over time (Fig. 1 B), it became evident that by day 4 after injection of OBs, divided $CD4^+$ T cells appeared in the nondraining nodes as well as the spleen. These T cells had divided at least three to four times and expressed high levels of CD44 while having down-regulated the early activation marker CD69, which is consistent with an activated phenotype, as previously reported (Lambrecht et al., 2000; unpublished data). Strikingly, these divided cells could also be traced back to the lung interstitium (by flow cytometry; Fig. 1 C), where they were found surrounding the injected OBs (by confocal imaging and immunostaining for DO11.10 TCR; Fig. 1 D). Some OVA-specific DO11.10 T cells were seen in immediate proximity of lung vessels in the vicinity of OBs, suggesting a specific recruitment mechanism at this site. When the immune response was evaluated even later (days 8 and 16), it was clear that divided $CD4^+$ T cells could no longer be traced back in the LNs, spleen, or lung, suggesting that they were deleted or their numbers had declined to a level below the threshold of detection by flow cytometry (Fig. 1 B).

Although these findings certainly suggested that there is a mechanism of immune induction for Ag trapped in the lung vasculature, these experiments were not conclusive as to

OVA-specific T cells could be found in close proximity to blood vessels (BV) and around the OB. Bars, 40 μm. (E) Whole particulate Ag is cross-presented in draining MLNs of the lung. At day −2, OVA-specific Tg $CD8^+$ CFSE-labeled OT-I were injected i.v., and at day 0, OBs (LPS free) or UBs were injected i.v. At day 4, MLNs were gated on CD8 T cells and analyzed for division CFSE profile (x axis) of Vβ5.1/5.2–PE-positive OVA-specific T cells (y axis). This experiment was performed three times with four mice per group. (F) Whole particulate Ag is presented in draining MLNs of the lung. Division CFSE profiles (x axis) of $CD4^+$ Vβ5.1/5.2–PE-positive (y axis) OT-II OVA-specific T cells in MLNs, 4 d after OB injection. Cells were gated for CD4 positivity. This experiment was performed three times with four mice per group. (G) Size of inflammation surrounding UBs or OBs in the lung as measured by image analysis measuring at days 4, 8, and 16 after injection of UBs (white bars) and OBs (black bars). Groups consisted of five mice at each day point. The experiment was performed three times. Mean ± SEM of the group is depicted. *, $P < 0.05$.

whether Ag would also be processed, as beads were coated with preprocessed OVA peptide. We therefore also studied whether whole OVA protein coupled to Sepharose beads would be processed and presented to CD4 and cross-presented to CD8 T cells. We therefore turned to the C57BL/6 background, in which both CD4 (OT-II) and CD8 (OT-I) TCR Tg mice are available (Barnden et al., 1998). For this, C57BL/6 mice received MHCI-restricted OT-I or MHCII-restricted OT-II OVA TCR Tg T cells. In both circumstances, we observed T cell divisions in the MLNs 4 d after injection of OBs (Fig. 1, E and F). Again, injection of OBs did not lead to T cell divisions outside the draining area of the lung (unpublished data).

In the lungs, we followed the size of the inflammatory lesions surrounding OBs or UBs. By day 4 of the response, the inflammatory lesions (as measured by the mean surface area of the inflammation minus the surface area of the bead divided by the bead surface area [see Materials and methods]) was greatly enhanced in mice receiving OBs compared with UBs. However by days 8–16, all inflammation surrounding the beads had disappeared, illustrating the transient nature of lung inflammatory lesions (Fig. 1 G). Together, these data suggested the presence of an active immune surveillance mechanism in the lung vascular bed that was induced in the mediastinal nodes.

Monocyte-derived DCs accumulate around particulate Ag trapped in the lung vasculature

We next addressed by which mechanism trapped Ag would be presented in the lung vascular bed. First, we studied the distribution of injected beads after i.v. injection. Injected beads were found exclusively in the lung vascular bed (Fig. 2 A) but not in the draining MLN, nondraining LN, or spleen (not depicted). As there was Ag presentation in the MLN, despite absence of macroscopic beads at this site, we reasoned that a migratory APC population might carry antigenic cargo to the node. As soon as 6 h after injection of UBs or OBs, we detected a population of $CD11c^+$ cells around the injected beads, irrespective of whether beads were coated with OVA peptide (Fig. 2 A, days 1–16) or not (not depicted). In addition, MHC class II^+ cells started to appear around these beads around this time period. Double staining revealed these cells to be $CD11c^+$ and MHC class II^+ double positive, strongly suggesting they were DCs (Fig. 2 A). When followed over time, the number of $MHCII^+CD11c^+$ cells was increased at day 4 after injection of OBs compared with injection of UBs, a time point when inflammatory lesions and accumulation of $CD4^+$ T cells were also maximal (Fig. 2 B). Later in the response, $CD11c^+$ DCs were still present around OBs but, gradually, their numbers decreased. To check for the presence of myeloid cells (like monocytes, neutrophils, and some DC subsets), we also stained for the presence of $CD11b^+$ cells. We found $CD11b^+$ cells to be abundantly present around OBs (Fig. 2 A, bottom).

The CD11c integrin is expressed on different cell types in the mouse lung but is mainly restricted to $CD11b^+$ and $CD11b^-$ conventional lung DCs, inflammatory type $CD11b^+$ DCs, and $CD11b^-$ alveolar macrophage in the lung (de Heer et al., 2004; van Rijt et al., 2004; Vermaelen and Pauwels, 2004; Sung et al., 2006; GeurtsvanKessel et al., 2008). Lung plasmacytoid DCs (pDCs) are characterized by intermediate expression of CD11c and expression of Gr1 (Ly6G/C), B220, and the specific marker BST2 (recognized by the mAb 120G8; Asselin-Paturel et al., 2003; de Heer et al., 2004, 2005). To analyze which subset of $CD11c^+$ DC was recruited to particulate Ag, frozen sections were stained with CD11c and Gr1 (recognizing Ly6C/G) or B220. Remarkably, $CD11c^+$ cells surrounding beads were $Gr1^+$ but lacked expression of the B220 marker, which is normally expressed on the surface of pDCs (Fig. S2). We also stained for pDCs by using the pDC-specific antibody 120G8, and this staining confirmed that $Gr1^+$ $CD11c^+$ DCs were not pDCs (unpublished data). We did not observe significant amounts of CD103, which is found on a subset of $CD11b^-$ lung DCs (unpublished data).

The expression of Gr1 (Ly6G/C) on lung $CD11c^+$ cells surrounding beads was unexpected, as this marker is classically not found on lung DCs in steady state (GeurtsvanKessel and Lambrecht, 2008; GeurtsvanKessel et al., 2008). Gr1 also recognizes the Ly6C Ag, expressed on a subset of monocyte-derived inflammatory DCs (Randolph et al., 1999; Geissmann et al., 2003; Sunderkötter et al., 2004; León et al., 2007; León and Ardavín, 2008). In the mouse, circulating monocytes can be discriminated into $Ly6C^+$ $CX3CR1^{int}$ $CD11b^+$ monocytes and $Ly6C^-$ $CX3CR1^{hi}$ $CD11b^+$ monocytes (Geissmann et al., 2003). Several groups have now shown that both types of monocytes are immediate circulating precursors for lung DCs but not steady-state lymphoid tissue conventional DCs (Geissmann et al., 2003; Landsman et al., 2007; Varol et al., 2007; Jakubzick et al., 2008).

To test the presence and differentiation of monocytes around injected beads at earlier time points, we injected $CX3CR^{GFP}$ mice with OBs (Jung et al., 2000). In these $CX3CR^{GFP}$ mice, all monocytes (and some T cells and NK cells) can be identified by GFP positivity and precisely localized in tissues using confocal imaging. As shown in Fig. 2 C, 6 h after injection of OBs, $CX3CR^{GFP+}$ cells were seen around injected beads. At the same time, $Ly6C^+$ and $CD11c^+$ cells were seen. The majority of cells were triple positive. It is of note that few cells were $CX3CR1^+Ly6C^-$, signifying resident blood monocytes, although some cells expressed CX3CR1 and Ly6C without CD11c, representing recruited inflammatory monocytes (Auffray et al., 2007).

Monocyte-derived DCs are necessary and sufficient for presentation of particulate Ag trapped in the lung vasculature

These findings of Ag presentation in the MLN draining the lungs and accumulation of $Ly6C^+CD11c^+$ cells around injected beads suggested that DCs were the major APC population presenting bead-associated intravascular Ag to T cells. To address the precise contribution of $CD11c^+$ DCs, we used

mice expressing the human diphtheria toxin (DT) receptor (DTR) under the control of the murine CD11c promotor, allowing the DT-induced conditional depletion of all conventional CD11c$^+$ DCs but leaving pDCs largely unaffected (Jung et al., 2002; Sapoznikov et al., 2007). We administered DT i.p. at the time of OB injection and followed the division of CFSE-labeled DO11.10 T cells. As seen in Fig. 3 A, T cell proliferation at day 4 of the response in the MLNs of CD11c-DTR Tg mice given DT was dramatically reduced to the level seen in mice given UBs. However, non-Tg littermate control mice given DT (or CD11c-DTR Tg mice given PBS [unpublished data]) still mounted a normal response to bead injection. The reduction of T cell proliferation in DC-depleted mice was accompanied by a severe reduction in the size of the inflammatory lesions surrounding the OBs at day 4 after injection (unpublished data). To study if DT treatment depleted local CD11c$^+$ cells around injected beads, we perfomed immunostaining for CX3CR1, Ly6C, and CD11c. Whereas in DTR-Tg mice given PBS treatment there was a clear recruitment of triple-positive cells 24 h after injection of OBs, these cells were severely reduced by DT treatment. Very strikingly, the depletion of CD11c^{hi} cells using DT also led to a reduction in CX3CR$^+$Ly6C$^+$CD11c$^-$ inflammatory monocytes (Fig. 3 B). As the depletion of these monocytes in CD11cDTR Tg mice has never been demonstrated before and as these cells lack expression of CD11c, whose promotor is driving DTR expression, we hypothesized that DT treatment led to a reduction of inflammatory monocytes indirectly. It has been shown that CD11c$^+$ cells of the lungs are a predominant source of chemokines for recruitment of other inflammatory cell types (Beaty et al., 2007). In support of this hypothesis, we performed stainings for monocyte chemotactic protein 1 (MCP-1, also known as CCL2), the major chemokine recruiting CCR2^{hi} inflammatory monocytes (Fig. 3 C). In PBS-treated DTR-Tg mice given OBs, there was a strong signal for MCP-1 colocalizing with DAPI$^+$CD11c$^+$ cells and

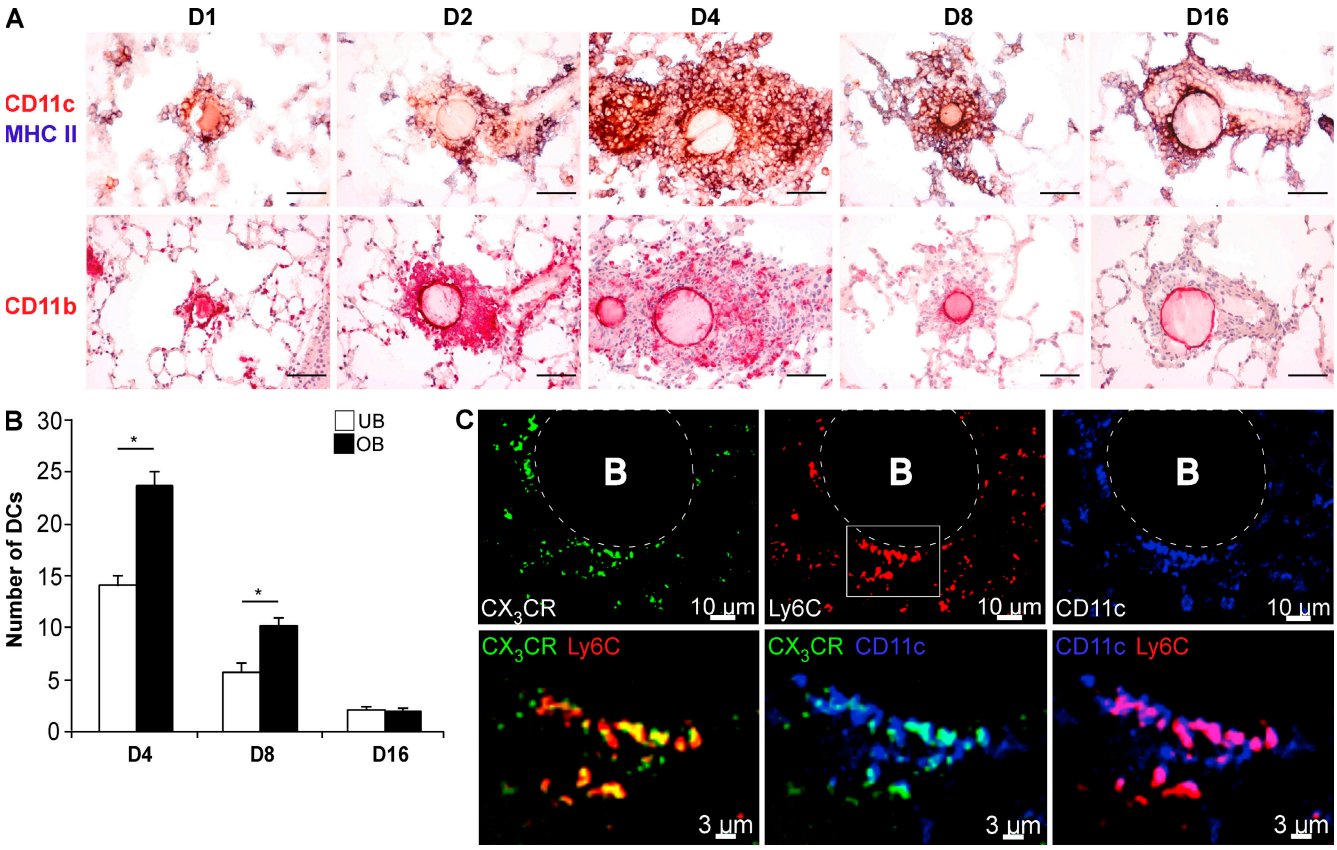

Figure 2. DCs and their monocytic precursors surround trapped particulate Ag. (A) 6-µm lung sections at 1, 2, 4, 8, and 16 d after injection of OBs were double stained for CD11c and MHC class II expression to identify the appearance of DCs around the particulate Ag. Furthermore, myeloid cells surrounding OB were stained with an anti-CD11b antibody on a consecutive slide. UBs are not shown in A but are summarized under B. This experiment was performed three times with four mice per group. Bars, 40 µm. (B) Absolute number of DCs surrounding OB and UB (double stained for CD11c$^+$ and MHCII$^+$) were counted for $n = 4$ mice per day per group. Results are shown as mean of CD11C$^+$MHCII$^+$ DCs of 30 separate lesions surrounding beads ± SEM. *, $P < 0.05$. This experiment was performed twice. (C) Presence of monocytic markers on CD11c$^+$ cells surrounding OBs. For this purpose, C57BL/6 CX3CR-GFP (green) Tg mice received OBs and OTII T cells. Lungs were sampled 6 h after OB i.v. injection. Slides were additionally stained for Ly-6C (red) and CD11c (blue). Beads are marked by dashed circles and a capital B. Overlays of a frame depicted in the top middle (rectangle) are shown in the bottom. This experiment was performed twice.

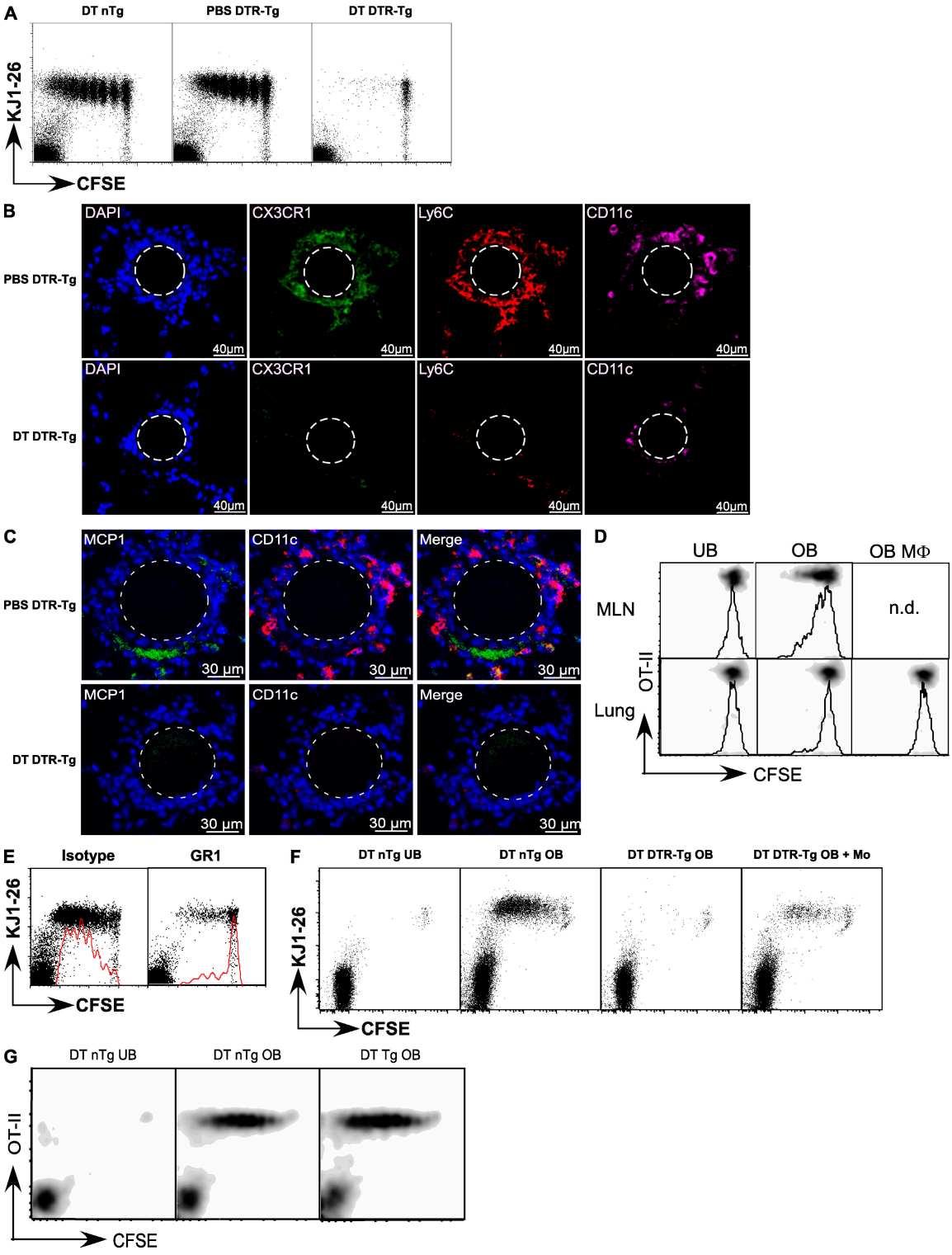

Figure 3. Monocyte-derived CD11c⁺ DCs are essential and sufficient for priming of naive CD4⁺ in lung draining MLNs in response to Ag trapped in the lung vasculature. (A) Effect of DT treatment in CD11c-DTR Tg mice on Ag presentation of large embolic Ag. At day 4 after injection of OB, hardly any division in CFSE-labeled DO11.10 OVA-specific CD4⁺ T cells could be found in draining lung MLNs in DT-treated DTR-Tg mice, whereas strong divisions were seen at that same time point in non-Tg littermates mice receiving OB and DT or DTR-Tg mice receiving OB and PBS as a control treatment. (B) Effect of DT treatment on presence of monocytes and DCs around beads. 24 h after DT treatment, fewer CX3CR1⁺Ly6C⁺ monocytes and CX3CR1⁺Ly6C⁺ CD11c⁺ inflammatory DCs were found around injected OB in CD11c-DTR-Tg mice compared with PBS treatment. Beads are marked by dashed circles. (C) Effect of DT treatment on monocyte specific chemokines. CD11c⁺ cells were depleted with DT injection on day 0 in CD11c DTR-Tg mice.

a clear MCP-1 signal localized to the DAPI^{neg} extracellular space. However in DT-treated DTR-Tg mice, both CD11c-associated and extracellular MCP-1 staining was abolished.

This data suggested that the effect of DT treatment on Ag presentation of bead-associated Ag could be the result of direct effects on resident DCs or to indirect effects on recruited monocytes that subsequently differentiate to infammatory type DCs. To further study the contribution of inflammatory DCs in presentation of large embolic Ag, we sorted Ly6C$^+$ CD11b$^+$CD11c$^+$ inflammatory DCs from the MLN and lungs 24 h after injection of OB or UB (Fig. 3 D). Whereas lung-derived inflammatory DCs did not present the OVA to CD4 T cells, MLN derived inflammatory DCs readily did. Similar experiments using CD8 OVA-specific T cells as a read out demonstrated that both MLN and lung inflammatory DCs presented to CD8 T cells (Fig. S3). In contrast, autofluorescent F4/80$^+$CD11c$^+$ alveolar macrophages did not present the Ag to CD4 or CD8 T cells (Fig. 3 D and Fig. S3). Cells with this phenotype were not seen to migrate to the MLN.

To more directly address the functional role of Ly6C$^+$ monocytes and their offspring in causing T cell proliferation after i.v. injection of embolic Ag, we performed depletion experiments in which monocytes were depleted using the Gr1 (Ly6C/G) antibody (Jakubzick et al., 2008). Single injection treatment with this antibody did not affect the number of lung-resident DC subsets (unpublished data). At day 4, mediastinal T cell division was severely reduced in Gr1-treated mice, compared with isotype-treated mice (Fig. 3 E), almost down to the level of mice injected with UBs (not depicted). The formation of inflammatory lesions around injected OB was also significantly suppressed and delayed until day 8 after injection of beads in mice depleted of Gr1$^+$ cells compared with the control isotype-treated mice, which had the maximum inflammatory lesions at day 4 (Fig. S4 A). However, by day 16, all inflammatory lesions had cleared, even in Gr1-treated mice. The Gr1 antibody has also been used to deplete pDCs from the lungs of mice (de Heer et al., 2004; Smit et al., 2006). To address the specific contribution of pDCs in this response, we also treated mice with the depleting antibody 120G8, recognizing the more pDC-restricted Ag bone marrow stromal Ag 2 (Asselin-Paturel et al., 2003). The treatment with 120G8 around injection of OBs did not affect the degree of T cell proliferation in draining MLNs at day 4 of the response, compared with isotype-treated mice (Fig. S4 B), nor did it affect the size of inflammatory lesions (not depicted).

As these experiments in CD11c$^+$-depleted and Gr1-treated mice clearly demonstrated that these cells were necessary for immune induction in the lung capillary filter, we next questioned if Ly6C$^+$ monocytes would also be sufficient for inducing an immune response to Ag trapped in the lung vasculature. For this purpose, Ly6C^{hi} monocytes were sorted from the bone marrow (based on expression of CD11b and Ly6C and lack of expression of CD31) and adoptively transferred i.v. in CD11c DTR Tg mice given DT around the time of bead injection. As seen in Fig. 3 F, restoration of OVA-specific CD4$^+$ T cell divisions could be accomplished by injection of bone marrow–purified Ly6C^{hi} monocytes.

Monocytes have also been shown to be precursors of Langerin$^+$ DCs in the lungs (Jakubzick et al., 2008) and Langerhans cells of the skin (Ginhoux et al., 2006), and DT treatment of CD11c-DTR might target these langerin$^+$ DCs directly, as they express high levels of CD11c. Therefore, we also addressed whether lung langerin$^+$ DCs were involved in this response by treating C57BL/6 langerin-DTR mice systemically with DT. In these mice, depletion of langerin$^+$ cells had no effect whatsoever on divisions of OVA-specific OTII T cells in the MLNs, which is in sharp contrast to the same treatment in CD11cDTR mice (Fig. 3 G). Together, these data therefore suggest that venous embolic Ags are filtered in the lung vascular bed and presented by monocyte-derived CD11c$^+$ DCs in the MLNs.

Induction of maturation of monocyte-derived DCs by microbial stimuli and trimeric CD40L increases effector potential of T cells without affecting T cell division

In all our experiments, we observed that inflammatory lesions around the OBs eventually resolved by day 8 of the response. This could be a result of the fact that OBs are seen as relatively harmless Ags, leading to a failure of functional maturation in monocyte-derived CD11c$^+$ DCs. To address this point, mice were injected with OBs that were also coated or not with LPS and/or trimeric CD40L or as a control with UBs. Trimeric CD40L is an effective agonist of CD40 on DCs and is known to induce DC maturation, particularly when a concomitant TLR agonist such as endotoxin is administered (Schulz et al., 2000). In mice receiving OB coated in combination with trimeric CD40L and LPS, there was a

24 h after DT treatment and OB injection, no MCP-1 was found around injected beads, whereas in PBS-treated Tg mice, MCP-1 was found colocalizing with CD11c and in the extracellular space not containing DAPI$^+$ nuclei. Beads are marked by dashed circles. (D) DCs and macrophages were sorted from MLN and lung from mice injected with UB or OB. These APCs were subsequently put in co-culture with CFSE-labeled OT-II cells for 4 d. Autofluorescent alveolar macrophages were not detected (n.d.) in the MLNs. (E) Effect of depletion of Ly6C/G cells using Gr1 antibody. CFSE-labeled OVA-specific CD4$^+$ DO11.10 division profile in draining MLNs in mice treated with anti-Gr1 or isotype i.p. at day 0 and injected with OB, measured at day 4. (F) Ly6C^{hi} monocytes restore T cell division in CD11c-depleted mice. CD11c/DTR-Tg mice or non-Tg littermates (nTg) received CFSE-specific OVA-specific CD4$^+$ T cells at day −2, with DT at day 0, with either UB (nTg) at day 0 or OB (nTg) at day 0, or OB at day 0 (DTR-Tg mice) with or without 3.5×10^5 bone marrow–purified (>99%) Ly6C^{hi} CD11b^{hi} monocytes. CD4$^+$ OVA-specific T cell divisions in these groups are shown in draining MLNs at day 4 after UB or OB injection. DTR-Tg mice depleted of CD11c$^+$ by DT show reconstitution of divisions by monocyte i.v. injection at day 0. (G) Depletion of langerin$^+$ lung DCs, using DT injection, in langerin-DTR mice showed no effect on OVA-specific T cell proliferation, compared with nTg mice given DT. These experiments were performed two to five times with five mice per group per time point.

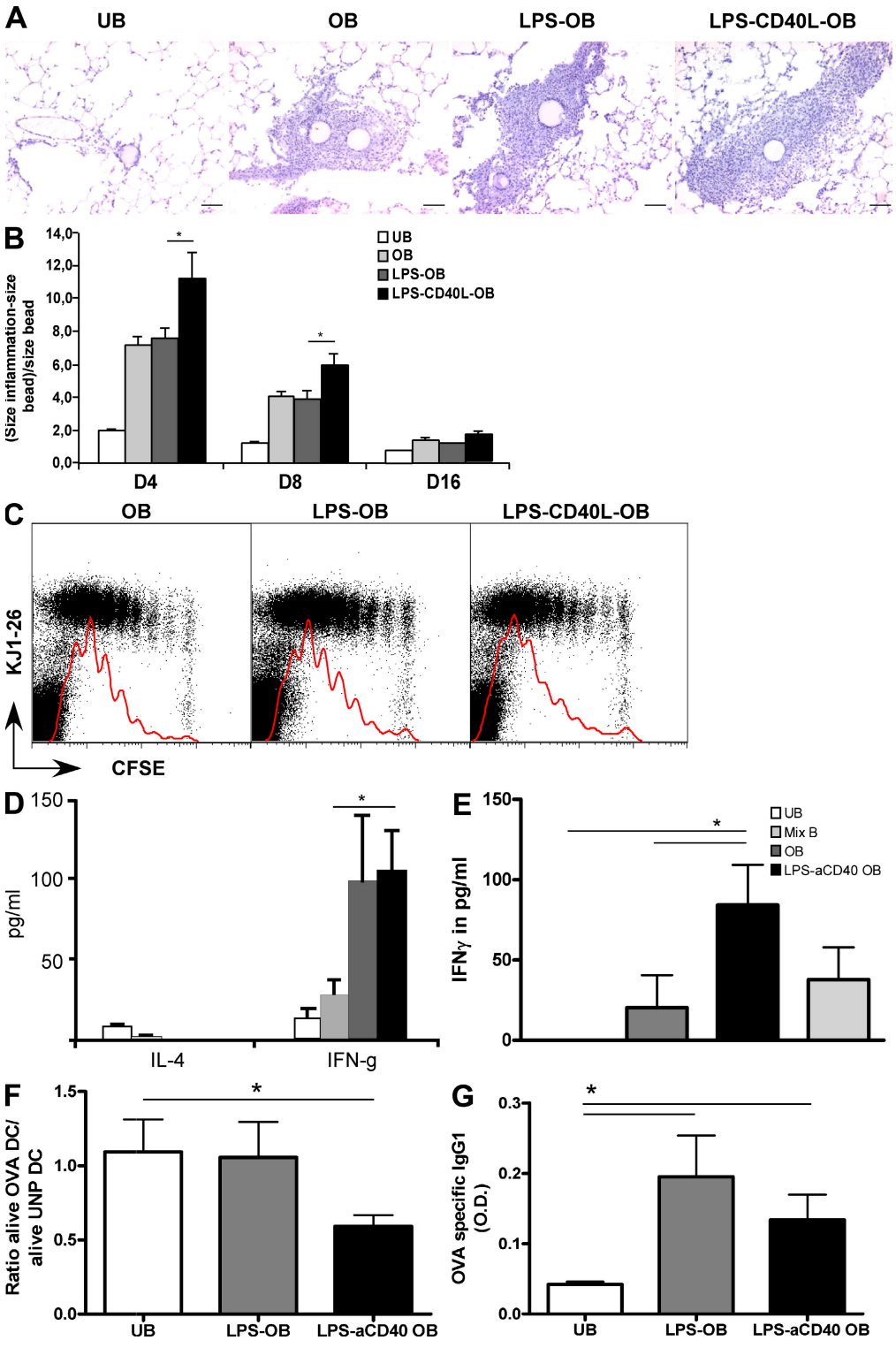

Figure 4. Effect of triggering TLR4 receptor and CD40 on Ag presentation to Ag trapped in the lung vasculature. (A) Mice received OVA-specific CD4+ DO11.10 T cells at day −2, and UBs, OBs, OB co-coated with LPS (LPS-OB), or OB co-coated with LPS and trimeric CD40L (LPS-CD40L-OB) at day 0. 4 d later, inflammation surrounding the beads is shown in these groups. Bars, 100 µm. (B) Size of inflammation surrounding the beads in the lungs in these groups is shown at days 4, 8, and 16. Data are shown as mean (n = 4 mice/group) ± SEM. *, $P < 0.05$. (C) Representative flow cytometry analyses of (n = 4 per group) OVA-specific CD4+ T cell divisions in draining lung MLNs at day 4 are shown. (D) Cytokine production in cultures of MLN, restimulated for 4 d in the presence of OVA Ag. The level of IL-4 was at the detection limit of the IL-4 ELISA (15 ng/ml). *, $P < 0.05$. Error bars represent statistical significance between these groups. (E) IFN-γ production by T cells was also analyzed in supernatant of restimulated MLN cells, from mice injected with 3 ×

strong increase in the size of inflammatory lesions around the OBs (Fig. 4 A, inflammatory lesions at day 4 after bead injection). LPS co-coating of OB by itself was insufficient to obtain this effect (Fig. 4, A and B). This enhancing effect was maintained until day 16 after injection of beads, although inflammatory lesions became much smaller compared with those seen on day 4 (Fig. 4 B). Despite the occurrence of larger inflammatory lesions around OBs with LPS and sCD40L, at day 16 all inflammatory lesions were again resolved. Provision of these DC-maturing stimuli did not affect the strength of T cell divisions in the MLN at day 4 after OB injection (Fig. 4 C). When the amount of cytokine production was measured in cultures of MLN, restimulated for 4 d in the presence of OVA Ag, the addition of LPS and/or sCD40L clearly enhanced the production of IFN-γ, whereas IL4 remained at the detection limit of the ELISA (Fig. 4 D). To address whether CD40 and TLR4 triggering had to occur physically on the same particulate OB, mice received beads coated simultaneously with OVA, LPS, and anti-CD40 or mice received beads coated separately with OVA, LPS, or anti-CD40. OB and LPS-aCD40 OB-injected mice also received 2/3 UB to equalize the amount of beads and the amount of OVA Ag given between groups. As shown in Fig. 4 E, restimulated MLN cells secreted more IFN-γ when the beads were coated with OVA, LPS, and α-CD40 simultaneously, compared with mice given a mixture of separately labeled OB, anti-CD40 beads, and LPS beads. We also addressed whether injection of OBs in conjunction with CD40 and TLR4 triggering led to induction of CTL responses to OVA-pulsed target cells. For this, we injected an equal amount of OVA-pulsed or unpulsed BM-DC targets, stained, respectively, with CMTMR and CFSE (Ritchie et al., 2000). As shown in Fig. 4 F, simultaneous triggering of CD40 and TLR4 on beads led to induction of OVA-specific lytic effectors that killed 50% of injected OVA-pulsed DCs, whereas injection of UBs or OVA-LPS–coated beads did not have this effect. Finally we also addressed the induction of humoral OVA-specific immunity by injection of these beads. We observed induction of OVA-specific IgG_1 after injection of OBs already when only TLR4 was triggered, whereas injection of UBs did not induce OVA-specific antibodies.

DISCUSSION

In this paper, using a system of traceable Ag-reactive T cells specific to OVA, we report that the meshwork of small lung vessels allows the effective filtering of large embolic Ags followed by uptake of the Ag by monocyte-derived $CD11c^+$ DCs and Ag presentation to $CD4^+$ and $CD8^+$ T cells in the MLNs. Primed T cells subsequently return to the lung and form short-lived inflammatory lesions that are ultimately cleared. This response clearly depends on $Ly6C^+$ monocytes and $CD11c^{hi}$ DCs, as it is eliminated in mice with a conditional deletion of $CD11c^+$ cells and depleted of Gr1 $(Ly6C/G)^+$ cells, and restored by adoptive transfer of $Ly6C^{hi}$ monocytes (Jung et al., 2002). These data, therefore, identify a third filtering network for bloodborne Ags, in addition to the spleen and liver, that is specialized for immune induction against large embolic material.

Strikingly, early after injection of embolic material, there was an accumulation $CD11c^+MHCII^+$ DCs surrounding the injected beads of which the origin can be debated. One possibility is that the resident interstitial DCs of the lung that can be found in alveolar septa would migrate to the occluded vessels and sample the vessel content. Numerous studies in mouse and rat have indeed demonstrated that alveolar septa contain DCs in close proximity to small diameter arterioles and alveolar capillaries (Sertl et al., 1986; Holt et al., 1988, 1992). However, these interstitial DCs have classically been described as sessile cells that fail to migrate to draining LNs and would merely restimulate already primed T cells during pulmonary delayed-type hypersensitivity–like reactions (Kradin et al., 1993; von Garnier et al., 2005). Another possible explanation would be that DCs accumulated on the injected beads from within the vessel lumen. Pulmonary vessels already contain a large marginating pool of DC precursors, possibly hardwired for Ag recognition at this site. This has been suggested by Suda et al. (1998), who demonstrated that the blood cannulated from the lungs of rats contained much more DC precursors than vena cava–cannulated blood, and these cells obtained DC potential after culture in appropriate cytokines. Whether this sequence of DC differentiation from vascular precursors would occur in our system remains to be shown.

Although all of these scenarios are not mutually exclusive, we favor a third potential source for bead-associated $CD11c^+$ DCs. Ag presentation in our system of i.v. embolization occurred as the result of Ag recognition by $Gr1^+$ (Ly6C/G) $CD11c^+$ cells that accumulated as early as 6 h after bead injection. These cells most likely represented monocyte-derived DCs and not pDCs, as they lacked expression of B220 and 120G8. The evidence for this comes from the coexpression of the fractalkine (CX3CR) receptor, Ly6C, and CD11c on these cells and the fact that T cell proliferation and development of inflammatory lesions in the lung were significantly reduced when mice were depleted of Gr1 $(Ly6G/C)^+$ cells but not by

10^3 UB, 10^3 OB combined with 2×10^3 UB, 10^3 LPS-aCD40 OB combined with 2×10^3 UB, or mixed beads. The mice receiving mixed beads were injected with 10^3 OB, 10^3 LPS-B, and 10^3 α-CD40-B. Therefore, all mice received the same number of beads and the same amount of Ag. *, $P < 0.05$. Error bars represent statistical significance between these groups. (F) To analyze the OVA-specific effector T cell function in this model, mice were injected with UB, OB, or LPS–α-CD40-OB and, after 6 d, injected subcutaneously with OVA peptide–pulsed DCs mixed with unpulsed DCs, respectively CMTMR and CFSE labeled. This graph shows the ratio of alive OVA peptide DCs versus unpulsed DCs, 4 d after injection of target DCs. *, $P < 0.05$. Error bars represent statistical significance between these groups. (G) In serum of these mice, OVA-specific IgG_1 levels were measured by ELISA. *, $P < 0.05$. Error bars represent statistical significance between these groups. These experiments were done three times with five mice per group.

depletion of 120G8$^+$ cells. In previous studies, Ly6C$^+$ monocytes have been shown to be precursors for inflammatory-type DCs, thus acquiring APC function and expression of the CD11c marker, and most likely represent the immediate precursor to nature's adjuvant, the immunogenic DC (Serbina et al., 2003; Le Borgne et al., 2006; Naik et al., 2006; León et al., 2007; Shortman and Naik, 2007; Kool et al., 2008). In the mouse, circulating monocytes can be discriminated into Ly6C$^+$ CX3CR^{int} CD11b$^+$ inflammatory monocytes and Ly6C$^-$ CX3CR^{hi} CD11b$^+$ monocytes (Geissmann et al., 2003). Several groups have now shown that both types of monocytes are also immediate circulating precursors for lung DCs but not steady-state lymphoid tissue DCs (Geissmann et al., 2003; Landsman et al., 2007; Varol et al., 2007; Jakubzick et al., 2008). Strikingly, Ly6C^{hi} monocytes express the CCR2 receptor for MCP-1. Although we have not measured the level of this chemokine, others using an injection model of Schistosomal egg antigen or *Mycobacterium* purified protein derivate (PPD)–coated Sepharose beads could measure an early production of this chemokine by lung structural cells (Hogaboam et al., 1999). Supporting a crucial role for inflammatory monocytes in early granuloma formation, CCR2-deficient mice had a defect in early (day 1–2) granuloma formation. It will be interesting to study whether these CCR2-deficient mice also have a reduced DC accumulation around beads and delayed Ag presentation in our model. This could be a possibility, as CCR2 was shown to be crucial for DC recruitment to the other lung compartment, the airway mucosa, under inflammatory conditions (Robays et al., 2007). Alternatively, a population of CX3CR^{med} Ly6C$^-$ monocytes has been shown to patrol the inside of the vessel wall (Auffray et al., 2007; Geissmann et al., 2008) We do not believe, however, that this subset was involved in presenting trapped embolic Ag in the lung, as the majority of CX3CR^{gfp+} cells were Ly6C$^+$ and depletion of Gr1$^+$ cells abolished most Ag presentation, whereas adoptive transfer of Ly6C^{hi} monocytes restored it.

Systemic DT treatment of CD11c-DTR at the time of bead injection led to a reduction of CX3CR1$^+$Ly6C$^+$CD11c$^+$ DCs and inflammatory CX3CR1$^+$Ly6C$^+$CD11c$^-$ monocytes around injected OB. These findings were very striking, as injected DT only kills cells expressing high level CD11c and circulating monocytes with this phenotype have not been described to be depleted in these mice (Geissmann et al., 2003; Landsman et al., 2007; Sapoznikov and Jung, 2008). The fact that DT has a very short half-life also did not support a model in which CD11c (and consequent DTR expression) was up-regulated on monocytes after recruitment to the beads, rendering monocytes sensitive to DT. We favor a model in which resident CD11c$^+$ DCs act as gatekeepers that chemoattract the inflammatory DCs, which, in their turn, are the true vehicles of immunity. In support of this, we found that CD11c$^+$ DCs were a predominant source of MCP-1, the major chemokine attracting CCR2$^+$ inflammatory monocytes. In CD11c-DTR Tg mice, treatment with DT largely eliminated the presence of MCP-1 around the injected beads, explaining how DT treatment can also lead to a reduction in monocytes not expressing CD11c. Strikingly, a lot of the MCP-1 was found not associated with the DAPI nuclear signal. Previously, MCP-1 was found indeed to be able to mediate its chemotactic effects at a distance from its site of production, displayed on extracellular matrix proteoglycans (Palframan et al., 2001). However, the extracellular MCP-1 signal was completely eliminated in DC-depleted mice, suggesting that a CD11c^{hi} cell was the predominant source for extracellular MCP-1. The exact subtype of lung DCs expressing MCP-1 in our model remains to be established. Resident CD11c$^+$CD11b$^+$CD103^{neg} DCs are found in the lung interstitium and have been shown to be a prominent source of chemokines (Beaty et al., 2007). Recently also, Choi et al. (2009) identified a population of vascular CD11c$^+$ CD11b$^+$ cells that probes the large systemic vessels.

One surprising observation of this and other models of embolization, such as injection of *Schistosoma mansoni* soluble Ag-coated or *Mycobacterium* PPD Ag-coated Sepharose beads, was that inflammatory lesions around injected embolic material were very short lived (Chensue et al., 1994; Iyonaga et al., 2002). It is also known that parasites or parasite eggs that gain access to the venous system as part of their replicative cycle end up in the lung arterioles and capillaries, leading to formation of lung granulomas or transient pulmonary inflammatory infiltrates (called Löffler's syndrome). One explanation of these findings would be that, like in our model, monocyte-derived CD11c$^+$ DCs would not get the proper activation status to induce full blown effector cells, thus leading to a program of deletional proliferation of T cells. In support of this, IFN-γ cytokine production of dividing T cells of mice receiving OBs was not above the level seen in mice receiving UBs. Arguing against this possibility is the fact that injection of CD40 and LPS, two known activators of the DC system and its potential to produce IL12p70 (Schulz et al., 2000), enhanced the size of the inflammatory lesions, production of IFN-γ by dividing T cells, production of IFN-γ by tissue-infiltrating T cells, and lytic activity of CD8 CTLs, but eventually these were still cleared from the lung. Also, models in which PPD-coated beads or *S. mansoni* eggs are injected would lead to full DC activation, but still these granulomata are cleared eventually (Iyonaga et al., 2002). Such a system to clear the lung interstitial tissue of overt inflammatory lesions makes evolutionary sense as this is the site of vital gas exchange (Lambrecht, 2006). Several mechanisms in the lung, such as the suppressive function of the nearby alveolar macrophage with its secretion of antiinflammatory factors, such as TGF-β, IL1-RA, IL-10, and prostaglandins, might keep inflammation in check by down-regulating the Ag-presenting capacity of DCs (Holt et al., 1988; Iyonaga et al., 2002). Alternatively, early fibrosis occurring around injected beads could effectively shield off the Ag so that it is further ignored by the immune system, eventually leading to apoptosis of T cells (Hogaboam et al., 1999).

In conclusion, we have provided evidence for a highly active Ag sampling mechanism for embolic material trapped in the small vessels of the lung that can potentially lead to the

generation of effector T cell responses when properly triggered. It is likely that this system developed during evolution to allow the immune system to effectively recognize large particulate Ags acquiring access to the venous blood by invasion, such as parasite eggs or worms, or after direct (traumatic) access to the bloodstream. When such Ags would be retained in the lungs without a possibility for Ag recognition, this could lead to a very effective way of pathogen immune subversion, as the spleen or liver, two other major sites of immune induction against blood particulate Ags, cannot access these large Ags and the pathogen could mutate during residence in the lung. It will be interesting to study whether certain pathogens take advantage of this system by blocking DC migration to the mediastinal nodes. It could also be that allogenic cells disrupted as a group of cells from freshly transplanted vascularized organs are presented via this route, as these vascularized grafts lack a direct connection with afferent lymph and the lung vascular bed is the first small vessel filter encountered. Clearly, this pathway of immune induction in the lung vasculature deserves further study.

MATERIALS AND METHODS

Mice. 6–8-wk-old female BALB/c (H-2^d) and C57BL/6 mice were purchased from Harlan. OVA-TCR Tg mice (DO11.10) on a BALB/c background, OT-II and OT-I OVA-TCR Tg mice on a C57BL/6 background, CD11c-DTR Tg mice on a BALB/c background, and Langerin DTR Tg mice on a C57bl/6 background (Bennett et al., 2005) were bred at Erasmus University (Rotterdam, Netherlands) and University of Ghent (Ghent, Belgium). CX3CR-GFP on a C57BL/6 background was a gift from S. Jung (Weizmann Institute of Science, Rehovot, Israel; Jung et al., 2000). Mice were housed under specific pathogen-free conditions at the animal care facility at Erasmus University. All of the experimental procedures used in this study were approved by the Erasmus University Committee of Animal Experiments and the Animal Ethics Committee of the University of Ghent.

Reagents and antibodies. $OVA_{323-339}$ peptide was obtained from Ansynth Service B.V. OVA protein was obtained from Worthington Biochemical Corporation. CNBr-activated Sepharose 4B beads were obtained from Sigma-Aldrich. CFSE and CellTracker Orange (CMTMR) were obtained from Invitrogen. FITC-labeled anti-Gr1 (RB6-8C5) and PE-labeled KJ1-26 (clonotypic OVA-TCR) were obtained from Invitrogen, PE-Labeled anti-B220 (RA3-6B2), CD8-α (Ly-2), Vβ5.1/5.2, and APC-labeled anti-CD4 (RM4-5) were purchased from BD. Unconjugated anti-CX3CR1 and goat anti–rabbit FITC were obtained from Acris Antibodies.

Intravascular injection of emboli. BALB/c or C57BL/6 mice received i.v. in the lateral tail vein 10^4 OVA-coated (OB) or noncoated (glycine; UB) CNBr-activated Sepharose 4B beads on day 0. Beads between 40 and 150 μm in diameter were prepared and coated with OVA, as described by others (Chensue et al., 1994), and were concentrated on a 40-μm cell strainer to remove smaller beads. Because of low OVA-TCR–specific naive T cell frequency in these wild type BALB/c mice, 10×10^6 live CFSE-labeled OVA-TCR Tg naive DO11.10 T cells were given i.v. 2 d before injection of the beads (day –2). OVA-specific TCR Tg T cells were collected from the lymphoid organs of naive 4–6-wk-old DO11.10, OT-I, or OT-II mice and stained with CFSE (Invitrogen), as previously described (de Heer et al., 2004).

In some experiments, to address the role of DC maturation, mice also received OB co-coated with LPS (LPS-OB; LPS obtained from Sigma-Aldrich) or OB co-coated with LPS and trimeric CD40L (2 μg/ml sCD40L, 100 ng/ml LPS; LPS-CD40L-OB). Agonistic anti-CD40 was used at 200 ng/ml. Trimeric CD40L was a gift from Amgen.

Detection of the primary T cell response to OB injection i.v. On days 1, 2, 4, 8, and 16, MLNs, PLNs (axillary), spleens, and lungs were removed, and individual cell suspensions were prepared as previously described (Lambrecht et al., 2000). Cell suspensions were stained either with antibodies to CD4, CD8, KJ1-26 (specific anti-TCR antibody for the TCR recognizing OVA peptide in I-A^d), or Vβ5.1/5.2. Propidium iodide (Sigma-Aldrich) was added for exclusion of dead cells before analysis of CFSE profiles on a FACSCalibur flow cytometer using CellQuest (BD) and FlowJo software (Tree Star, Inc.).

For measurement of cytokine responses, cell suspensions obtained from MLNs were cultured at 200,000 cells per well in the presence of 10 μg/ml OVA protein. IL-4 and IFN-γ were measured at day 4 by ELISA (BD).

Depletion of DCs and monocytes. In experiments to address the functional role of DCs in inflammation formation around beads, CD11c$^+$ cells were depleted by injecting 100 ng DT i.p. in CD11c-DTR Tg mice (van Rijt et al., 2005). The same dose is used in Langerin DTR mice to deplete the Langerin$^+$ cells. In experiments to address the functional role of pDCs, pDCs were depleted by 120G8 antibody injection (200 μg at the day of bead injection; provided by C. Asselin-Paturel, Shering-Plough, Dardilly, France; Asselin-Paturel et al., 2003). For monocyte depletion, anti-Gr1 i.p. injection was used, which was given at 200 μg on the same day of bead injection.

In experiments to address if monocytes could restore immune responses in the DT-treated CD11c-DTR Tg mice, 3.5×10^5 CD11b$^+$Ly-6C$^+$CD31$^-$ monocytes sorted from bone marrow of RAG2 $\gamma_c^{-/-}$ BALB/c mice (Geissmann et al., 2003) were injected i.v. on day 0 after OB or UB injection. To investigate whether DCs migrated to the draining LNs and present OVA, DCs were sorted from the MLN and lung from mice that were injected 4 d earlier with OB and control mice that were injected with UB. Macrophages were sorted from the lungs of these mice as a control of APCs.

DCs and macrophages were subsequently brought in and co-cultured for 4 d with CFSE-labeled OT-I and OT-II cells to analyze their presenting capacity. Monocytes, DCs, and macrophages were sorted on a cell sorter (FACS-ARIAII; BD).

CTL response. C57BL/6 mice were injected with 10×10^6 unlabeled OT-I T cells and, 2 d later, with UB, LPS-OB, or LPS-aCD40-OB. DCs were cultured for 6 d from bone marrow of C57BL/6 mice with GM-CSF. At day 6, half of the DCs were pulsed with OVA peptide (10 μM SIINFEKL) for 2 h. These cells were harvested and labeled with 10 μM CMTMR (10×10^6 cells/ml) according to the manufacturer's protocol (Invitrogen). The unpulsed DCs were harvested and fluorescently labeled with 10 μM CFSE. Both types of DCs were mixed in a 1:1 ratio and injected 6 d after the subcutaneous bead injection. After another 4 d, the inguinal LNs were dissected and the migrated CMTMR$^+$ DCs and CFSE$^+$ DCs were analyzed by FACS. Serum was collected from these mice and OVA-specific IgG_1 levels were detected with ELISA (BD).

Confocal microscopy. Confocal analysis was performed on 6-μm cryostat sections of lungs stained with anti-CX3CR1/goat anti–rabbit FITC (Acris Antibodies), anti-Gr1 FITC, anti-B220 PE, Ly-6C biotin-streptavidin Alexa Fluor 555, CD11c Alexa Fluor 647, rabbit anti-MCP-1 (Abcam)/donkey anti–rabbit Cy3 (Jackson ImmunoResearch Laboratories, Inc.), and 120G8 coated with Quantum dots (Micro Probe, Inc.). Sections were collected on a confocal laser microscope (LSM-710; Carl Zeiss, Inc.) and analyzed using Imaris 5.0 software (Bitplane).

Immunohistochemistry and analysis of inflammation surrounding beads. For immunohistochemistry analysis of the inflammation, 6-μm cryostat sections of lungs were stained with CD11c, CD11b, and MHCII. For inflammation size, hematoxylin-counterstained lungs were analyzed with an image analysis system (Quantimed; Leica), whereby 30 beads per mice were measured, dividing the surface size of the bead (in micrometers squared) by the surface size of inflammation and bead together (in micrometers squared). 30 beads were chosen to attain a mean bead diameter, as slides were 6 μm.

Online supplemental material. Fig. S1 shows T cell divisions in spleen and draining LNs of the lung, liver, and periphery at days 2 and 4 after bead injection. Fig. S2 depicts a confocal image of a section of a lung 24 h after bead injection, stained with CD11c, GR1, and B220. Fig. S3 shows in vitro T cell proliferations of OT-I cells co-cultured with sorted DCs and macrophages from MLN and spleen 24 h after beads injection. In Fig. S4, the analysis of the size of the infiltrates after GR1 depletion, as well as the T cell proliferations after pDC depletion at day 4 after bead injection, is depicted. Online supplemental material is available at http://www.jem.org/cgi/content/full/jem.20082401/DC1.

The authors wish to thank W.A. van Cappellen for assistance with confocal microscopy.

H.J. de Heer was supported by an educational grant from AstraZeneca, The Netherlands, and B.N. Lambrecht and H. Hammad were supported by an Odysseus Grant of the Flemish government and by a concerted research initiative grant (GOA 01G01009) of Ghent University.

The authors have no conflicting financial interests.

Submitted: 24 October 2008
Accepted: 1 October 2009

REFERENCES

Asselin-Paturel, C., G. Brizard, J.J. Pin, F. Brière, and G. Trinchieri. 2003. Mouse strain differences in plasmacytoid dendritic cell frequency and function revealed by a novel monoclonal antibody. *J. Immunol.* 171:6466–6477.

Auffray, C., D. Fogg, M. Garfa, G. Elain, O. Join-Lambert, S. Kayal, S. Sarnacki, A. Cumano, G. Lauvau, and F. Geissmann. 2007. Monitoring of blood vessels and tissues by a population of monocytes with patrolling behavior. *Science.* 317:666–670. doi:10.1126/science.1142883

Banchereau, J., and R.M. Steinman. 1998. Dendritic cells and the control of immunity. *Nature.* 392:245–252. doi:10.1038/32588

Barnden, M.J., J. Allison, W.R. Heath, and F.R. Carbone. 1998. Defective TCR expression in transgenic mice constructed using cDNA-based alpha- and beta-chain genes under the control of heterologous regulatory elements. *Immunol. Cell Biol.* 76:34–40. doi:10.1046/j.1440-1711.1998.00709.x

Beaty, S.R., C.E. Rose Jr., and S.S. Sung. 2007. Diverse and potent chemokine production by lung CD11bhigh dendritic cells in homeostasis and in allergic lung inflammation. *J. Immunol.* 178:1882–1895.

Bennett, C.L., E. van Rijn, S. Jung, K. Inaba, R.M. Steinman, M.L. Kapsenberg, and B.E. Clausen. 2005. Inducible ablation of mouse Langerhans cells diminishes but fails to abrogate contact hypersensitivity. *J. Cell Biol.* 169:569–576. doi:10.1083/jcb.200501071

Chensue, S.W., K. Warmington, J. Ruth, P. Lincoln, M.C. Kuo, and S.L. Kunkel. 1994. Cytokine responses during mycobacterial and schistosomal antigen-induced pulmonary granuloma formation. Production of Th1 and Th2 cytokines and relative contribution of tumor necrosis factor. *Am. J. Pathol.* 145:1105–1113.

Choi, J.-H., Y. Do, C. Cheong, H. Koh, S.B. Boscardin, Y.-S. Oh, L. Bozzacco, C. Trumpfheller, C.G. Park, and R.M. Steinman. 2009. Identification of antigen-presenting dendritic cells in mouse aorta and cardiac valves. *J. Exp. Med.* 206:497–505. doi:10.1084/jem.20082129

de Heer, H.J., H. Hammad, T. Soullié, D. Hijdra, N. Vos, M.A. Willart, H.C. Hoogsteden, and B.N. Lambrecht. 2004. Essential role of lung plasmacytoid dendritic cells in preventing asthmatic reactions to harmless inhaled antigen. *J. Exp. Med.* 200:89–98. doi:10.1084/jem.20040035

de Heer, H.J., H. Hammad, M. Kool, and B.N. Lambrecht. 2005. Dendritic cell subsets and immune regulation in the lung. *Semin. Immunol.* 17:295–303. doi:10.1016/j.smim.2005.05.002

De Smedt, T., B. Pajak, E. Muraille, L. Lespagnard, E. Heinen, P. De Baetselier, J. Urbain, O. Leo, and M. Moser. 1996. Regulation of dendritic cell numbers and maturation by lipopolysaccharide in vivo. *J. Exp. Med.* 184:1413–1424. doi:10.1084/jem.184.4.1413

Feuerer, M., P. Beckhove, N. Garbi, Y. Mahnke, A. Limmer, M. Hommel, G.J. Hämmerling, B. Kyewski, A. Hamann, V. Umansky, and V. Schirrmacher. 2003. Bone marrow as a priming site for T-cell responses to blood-borne antigen. *Nat. Med.* 9:1151–1157. doi:10.1038/nm914

Geissmann, F., S. Jung, and D.R. Littman. 2003. Blood monocytes consist of two principal subsets with distinct migratory properties. *Immunity.* 19:71–82. doi:10.1016/S1074-7613(03)00174-2

Geissmann, F., C. Auffray, R. Palframan, C. Wirrig, A. Ciocca, L. Campisi, E. Narni-Mancinelli, and G. Lauvau. 2008. Blood monocytes: distinct subsets, how they relate to dendritic cells, and their possible roles in the regulation of T-cell responses. *Immunol. Cell Biol.* 86:398–408. doi:10.1038/icb.2008.19

GeurtsvanKessel, C.H., and B.N. Lambrecht. 2008. Division of labor between dendritic cell subsets of the lung. *Mucosal Immunol.* 1:442–450. doi:10.1038/mi.2008.39

GeurtsvanKessel, C.H., M.A. Willart, L.S. van Rijt, F. Muskens, M. Kool, C. Baas, K. Thielemans, C. Bennett, B.E. Clausen, H.C. Hoogsteden, et al. 2008. Clearance of influenza virus from the lung depends on migratory langerin^{+}CD11b^{-} but not plasmacytoid dendritic cells. *J. Exp. Med.* 205:1621–1634. doi:10.1084/jem.20071365

Ginhoux, F., F. Tacke, V. Angeli, M. Bogunovic, M. Loubeau, X.M. Dai, E.R. Stanley, G.J. Randolph, and M. Merad. 2006. Langerhans cells arise from monocytes in vivo. *Nat. Immunol.* 7:265–273. doi:10.1038/ni1307

Gong, J.L., K.M. McCarthy, R.A. Rogers, and E.E. Schneeberger. 1994. Interstitial lung macrophages interact with dendritic cells to present antigenic peptides derived from particulate antigens to T cells. *Immunology.* 81:343–351.

Hogaboam, C.M., C.L. Bone-Larson, S. Lipinski, N.W. Lukacs, S.W. Chensue, R.M. Strieter, and S.L. Kunkel. 1999. Differential monocyte chemoattractant protein-1 and chemokine receptor 2 expression by murine lung fibroblasts derived from Th1- and Th2-type pulmonary granuloma models. *J. Immunol.* 163:2193–2201.

Holt, P.G., M.A. Schon-Hegrad, and J. Oliver. 1988. MHC class II antigen-bearing dendritic cells in pulmonary tissues of the rat. Regulation of antigen presentation activity by endogenous macrophage populations. *J. Exp. Med.* 167:262–274. doi:10.1084/jem.167.2.262

Holt, P.G., J. Oliver, C. McMenamin, and M.A. Schon-Hegrad. 1992. Studies on the surface phenotype and functions of dendritic cells in parenchymal lung tissue of the rat. *Immunology.* 75:582–587.

Iyonaga, K., K.M. McCarthy, and E.E. Schneeberger. 2002. Dendritic cells and the regulation of a granulomatous immune response in the lung. *Am. J. Respir. Cell Mol. Biol.* 26:671–679.

Jakubzick, C., F. Tacke, F. Ginhoux, A.J. Wagers, N. van Rooijen, M. Mack, M. Merad, and G.J. Randolph. 2008. Blood monocyte subsets differentially give rise to CD103+ and CD103- pulmonary dendritic cell populations. *J. Immunol.* 180:3019–3027.

Jung, S., J. Aliberti, P. Graemmel, M.J. Sunshine, G.W. Kreutzberg, A. Sher, and D.R. Littman. 2000. Analysis of fractalkine receptor CX(3)CR1 function by targeted deletion and green fluorescent protein reporter gene insertion. *Mol. Cell. Biol.* 20:4106–4114. doi:10.1128/MCB.20.11.4106-4114.2000

Jung, S., D. Unutmaz, P. Wong, G. Sano, K. De los Santos, T. Sparwasser, S. Wu, S. Vuthoori, K. Ko, F. Zavala, et al. 2002. In vivo depletion of CD11c(+) dendritic cells abrogates priming of CD8(+) T cells by exogenous cell-associated antigens. *Immunity.* 17:211–220. doi:10.1016/S1074-7613(02)00365-5

Kool, M., T. Soullié, M. van Nimwegen, M.A. Willart, F. Muskens, S. Jung, H.C. Hoogsteden, H. Hammad, and B.N. Lambrecht. 2008. Alum adjuvant boosts adaptive immunity by inducing uric acid and activating inflammatory dendritic cells. *J. Exp. Med.* 205:869–882. doi:10.1084/jem.20071087

Kradin, R.L., W. Xia, K.M. McCarthy, and E.E. Schneeberger. 1993. FcR$^{+/-}$ subsets of Ia^{+} pulmonary dendritic cells in the rat display differences in their abilities to provide accessory co-stimulation for naive (OX-22^{+}) and sensitized (OX-22^{-}) T cells. *Am. J. Pathol.* 142:811–819.

Kudo, S., K. Matsuno, T. Ezaki, and M. Ogawa. 1997. A novel migration pathway for rat dendritic cells from the blood: hepatic sinusoids–lymph translocation. *J. Exp. Med.* 185:777–784. doi:10.1084/jem.185.4.777

Lambrecht, B.N. 2006. Alveolar macrophage in the driver's seat. *Immunity.* 24:366–368. doi:10.1016/j.immuni.2006.03.008

Lambrecht, B.N., R.A. Pauwels, and B. Fazekas De St Groth. 2000. Induction of rapid T cell activation, division, and recirculation by intratracheal injection of dendritic cells in a TCR transgenic model. *J. Immunol.* 164:2937–2946.

Landsman, L., C. Varol, and S. Jung. 2007. Distinct differentiation potential of blood monocyte subsets in the lung. *J. Immunol.* 178:2000–2007.

Le Borgne, M., N. Etchart, A. Goubier, S.A. Lira, J.C. Sirard, N. van Rooijen, C. Caux, S. Aït-Yahia, A. Vicari, D. Kaiserlian, and B. Dubois. 2006. Dendritic cells rapidly recruited into epithelial tissues via CCR6/CCL20 are responsible for CD8+ T cell crosspriming in vivo. *Immunity.* 24:191–201. doi:10.1016/j.immuni.2006.01.005

León, B., and C. Ardavín. 2008. Monocyte-derived dendritic cells in innate and adaptive immunity. *Immunol. Cell Biol.* 86:320–324. doi:10.1038/icb.2008.14

León, B., M. López-Bravo, and C. Ardavín. 2007. Monocyte-derived dendritic cells formed at the infection site control the induction of protective T helper 1 responses against Leishmania. *Immunity.* 26:519–531. doi:10.1016/j.immuni.2007.01.017

Millonig, G., H. Niederegger, W. Rabl, B.W. Hochleitner, D. Hoefer, N. Romani, and G. Wick. 2001. Network of vascular-associated dendritic cells in intima of healthy young individuals. *Arterioscler. Thromb. Vasc. Biol.* 21:503–508.

Morón, G., P. Rueda, I. Casal, and C. Leclerc. 2002. $CD8\alpha^-$ $CD11b^+$ dendritic cells present exogenous virus-like particles to $CD8^+$ T cells and subsequently express CD8α and CD205 molecules. *J. Exp. Med.* 195:1233–1245. doi:10.1084/jem.20011930

Naik, S.H., D. Metcalf, A. van Nieuwenhuijze, I. Wicks, L. Wu, M. O'Keeffe, and K. Shortman. 2006. Intrasplenic steady-state dendritic cell precursors that are distinct from monocytes. *Nat. Immunol.* 7:663–671. doi:10.1038/ni1340

Palframan, R.T., S. Jung, G. Cheng, W. Weninger, Y. Luo, M. Dorf, D.R. Littman, B.J. Rollins, H. Zweerink, A. Rot, and U.H. von Andrian. 2001. Inflammatory chemokine transport and presentation in HEV: a remote control mechanism for monocyte recruitment to lymph nodes in inflamed tissues. *J. Exp. Med.* 194:1361–1373. doi:10.1084/jem.194.9.1361

Perros, F., P. Dorfmüller, R. Souza, I. Durand-Gasselin, S. Mussot, M. Mazmanian, P. Hervé, D. Emilie, G. Simonneau, and M. Humbert. 2007. Dendritic cell recruitment in lesions of human and experimental pulmonary hypertension. *Eur. Respir. J.* 29:462–468. doi:10.1183/09031936.00094706

Randolph, G.J., K. Inaba, D.F. Robbiani, R.M. Steinman, and W.A. Muller. 1999. Differentiation of phagocytic monocytes into lymph node dendritic cells in vivo. *Immunity.* 11:753–761. doi:10.1016/S1074-7613(00)80149-1

Ritchie, D.S., I.F. Hermans, J.M. Lumsden, C.B. Scanga, J.M. Roberts, J. Yang, R.A. Kemp, and F. Ronchese. 2000. Dendritic cell elimination as an assay of cytotoxic T lymphocyte activity in vivo. *J. Immunol. Methods.* 246:109–117. doi:10.1016/S0022-1759(00)00300-8

Robays, L.J., T. Maes, S. Lebecque, S.A. Lira, W.A. Kuziel, G.G. Brusselle, G.F. Joos, and K.V. Vermaelen. 2007. Chemokine receptor CCR2 but not CCR5 or CCR6 mediates the increase in pulmonary dendritic cells during allergic airway inflammation. *J. Immunol.* 178:5305–5311.

Sapoznikov, A., and S. Jung. 2008. Probing in vivo dendritic cell functions by conditional cell ablation. *Immunol. Cell Biol.* 86:409–415. doi:10.1038/icb.2008.23

Sapoznikov, A., J.A. Fischer, T. Zaft, R. Krauthgamer, A. Dzionek, and S. Jung. 2007. Organ-dependent in vivo priming of naive $CD4^+$, but not $CD8^+$, T cells by plasmacytoid dendritic cells. *J. Exp. Med.* 204:1923–1933. doi:10.1084/jem.20062373

Schulz, O., A.D. Edwards, M. Schito, J. Aliberti, S. Manickasingham, A. Sher, and C. Reis e Sousa. 2000. CD40 triggering of heterodimeric IL-12 p70 production by dendritic cells in vivo requires a microbial priming signal. *Immunity.* 13:453–462. doi:10.1016/S1074-7613(00)00045-5

Serbina, N.V., T.P. Salazar-Mather, C.A. Biron, W.A. Kuziel, and E.G. Pamer. 2003. TNF/iNOS-producing dendritic cells mediate innate immune defense against bacterial infection. *Immunity.* 19:59–70. doi:10.1016/S1074-7613(03)00171-7

Sertl, K., T. Takemura, E. Tschachler, V.J. Ferrans, M.A. Kaliner, and E.M. Shevach. 1986. Dendritic cells with antigen-presenting capability reside in airway epithelium, lung parenchyma, and visceral pleura. *J. Exp. Med.* 163:436–451. doi:10.1084/jem.163.2.436

Shortman, K., and S.H. Naik. 2007. Steady-state and inflammatory dendritic-cell development. *Nat. Rev. Immunol.* 7:19–30. doi:10.1038/nri1996

Smit, J.J., B.D. Rudd, and N.W. Lukacs. 2006. Plasmacytoid dendritic cells inhibit pulmonary immunopathology and promote clearance of respiratory syncytial virus. *J. Exp. Med.* 203:1153–1159. doi:10.1084/jem.20052359

Suda, T., K. McCarthy, Q. Vu, J. McCormack, and E.E. Schneeberger. 1998. Dendritic cell precursors are enriched in the vascular compartment of the lung. *Am. J. Respir. Cell Mol. Biol.* 19:728–737.

Sunderkötter, C., T. Nikolic, M.J. Dillon, N. Van Rooijen, M. Stehling, D.A. Drevets, and P.J.M. Leenen. 2004. Subpopulations of mouse blood monocytes differ in maturation stage and inflammatory response. *J. Immunol.* 172:4410–4417.

Sung, S.S., S.M. Fu, C.E. Rose Jr., F. Gaskin, S.T. Ju, and S.R. Beaty. 2006. A major lung CD103 (alphaE)-beta7 integrin-positive epithelial dendritic cell population expressing Langerin and tight junction proteins. *J. Immunol.* 176:2161–2172.

Tsuchiya, T., K. Chida, T. Suda, E.E. Schneeberger, and H. Nakamura. 2002. Dendritic cell involvement in pulmonary granuloma formation elicited by bacillus calmette-guérin in rats. *Am. J. Respir. Crit. Care Med.* 165:1640–1646. doi:10.1164/rccm.2110086

van Rijt, L.S., H. Kuipers, N. Vos, D. Hijdra, H.C. Hoogsteden, and B.N. Lambrecht. 2004. A rapid flow cytometric method for determining the cellular composition of bronchoalveolar lavage fluid cells in mouse models of asthma. *J. Immunol. Methods.* 288:111–121. doi:10.1016/j.jim.2004.03.004

van Rijt, L.S., S. Jung, A. Kleinjan, N. Vos, M. Willart, C. Duez, H.C. Hoogsteden, and B.N. Lambrecht. 2005. In vivo depletion of lung $CD11c^+$ dendritic cells during allergen challenge abrogates the characteristic features of asthma. *J. Exp. Med.* 201:981–991. doi:10.1084/jem.20042311

Varol, C., L. Landsman, D.K. Fogg, L. Greenshtein, B. Gildor, R. Margalit, V. Kalchenko, F. Geissmann, and S. Jung. 2007. Monocytes give rise to mucosal, but not splenic, conventional dendritic cells. *J. Exp. Med.* 204:171–180. doi:10.1084/jem.20061011

Vermaelen, K., and R. Pauwels. 2004. Accurate and simple discrimination of mouse pulmonary dendritic cell and macrophage populations by flow cytometry: methodology and new insights. *Cytometry A.* 61A:170–177. doi:10.1002/cyto.a.20064

von Garnier, C., L. Filgueira, M. Wikstrom, M. Smith, J.A. Thomas, D.H. Strickland, P.G. Holt, and P.A. Stumbles. 2005. Anatomical location determines the distribution and function of dendritic cells and other APCs in the respiratory tract. *J. Immunol.* 175:1609–1618.